



# Ground-based stratospheric O<sub>3</sub> and HNO<sub>3</sub> measurements at Thule, Greenland: an intercomparison with Aura MLS observations

I. Fiorucci<sup>1</sup>, G. Muscari<sup>1</sup>, L. Froidevaux<sup>2</sup>, and M. L. Santee<sup>2</sup>

<sup>1</sup>Istituto Nazionale di Geofisica e Vulcanologia, Roma, Italy

<sup>2</sup>Jet Propulsion Laboratory, California Institute of Technology, Pasadena, California, USA

Correspondence to: I. Fiorucci (irene.fiorucci@ingv.it)

Received: 24 December 2012 – Published in Atmos. Meas. Tech. Discuss.: 25 March 2013

Revised: 31 July 2013 – Accepted: 5 August 2013 – Published: 23 September 2013

**Abstract.** In response to the need for improving our understanding of the evolution and the interannual variability of the winter Arctic stratosphere, in January 2009 a Ground-Based Millimeter-wave Spectrometer (GBMS) was installed at the Network for the Detection of Atmospheric Composition Change (NDACC) site in Thule (76.5° N, 68.8° W), Greenland. In this work, stratospheric GBMS O<sub>3</sub> and HNO<sub>3</sub> vertical profiles obtained from Thule during the winters 2010 (HNO<sub>3</sub> only), 2011 and 2012 are characterized and intercompared with co-located measurements of the Aura Microwave Limb Sounder (MLS) experiment. Using a recently developed algorithm based on Optimal Estimation, we find that the GBMS O<sub>3</sub> retrievals show good sensitivity (> 80 %) to atmospheric variations between ~ 17 and ~ 50 km, where their 1σ uncertainty is estimated to be the larger of ~ 11 % or 0.2 ppmv. Similarly, HNO<sub>3</sub> profiles can be considered for scientific use between ~ 17 and ~ 45 km altitude, with a 1σ uncertainty that amounts to the larger of 15 % or 0.2 ppbv. Comparisons with Aura MLS version 3.3 observations show that, on average, GBMS O<sub>3</sub> mixing ratios are biased negatively with respect to MLS throughout the stratosphere, with differences ranging between ~ 0.3 ppmv (8 %) and 0.9 ppmv (18 %) in the 17–50 km vertical range. GBMS HNO<sub>3</sub> values display instead a positive bias with respect to MLS up to 26 km, reaching a maximum of ~ 1 ppbv (10 %) near the mixing ratio profile peak. O<sub>3</sub> and HNO<sub>3</sub> values from the two datasets prove to be well correlated at all altitudes, although their correlations worsen at the lower end of the altitude ranges considered. Column contents of GBMS and MLS O<sub>3</sub> (from 20 km upwards) and HNO<sub>3</sub> (from 17 km upwards) correlate very well and indicate that GBMS measurements can provide valuable estimates of column interannual and seasonal variations for these compounds.

## 1 Introduction

Driven by increasing concerns about anthropogenic ozone reduction, microwave spectroscopy started to be employed in the early 1980s to study various stratospheric constituents involved in the ozone depletion processes (e.g., Parrish et al., 1988, 1992; de Zafra et al., 1987; Connor et al., 1987; Waters et al., 1993). Together with chlorine compounds, HNO<sub>3</sub> plays a key role in these processes. It is a primary reservoir for reactive nitrogen in the stratosphere and one of the main components of Polar Stratospheric Clouds (PSCs) which provide surfaces for heterogeneous chemical conversion of chlorine from its reservoir species (HCl, ClONO<sub>2</sub>) into highly reactive ozone-destroying forms (Cl, ClO) (Solomon, 1990).

Starting in 1993, observations of stratospheric O<sub>3</sub> and HNO<sub>3</sub> have been carried out by means of a Ground-Based Millimeter-wave Spectrometer (GBMS) at different sites in both hemispheres, at polar and mid-latitudes (e.g., de Zafra et al., 1997; Muscari et al., 2007; Santee et al., 2007). GBMS data have contributed to shed light on processes related to the global ozone decline and to the dramatic ozone loss occurring over the Antarctic continent every spring. In particular, in 1993 the GBMS provided the first quasi-continuous year-long data record of HNO<sub>3</sub> and O<sub>3</sub> vertical profiles in the heart of the south polar vortex showing the direct link between the appearance of PSCs and the rapid removal of HNO<sub>3</sub> from the lower stratosphere (de Zafra et al., 1997). Since then, a continuous monitoring of the stratospheric composition changes in response to the anthropogenic forcing (including ozone depleting substances release) has been carried out by the Network for the Detection of Stratospheric Change (NDSC), now Network for the Detection of Atmospheric Composition Change (NDACC). Microwave spectroscopy

has been used to measure different stratospheric trace gases since the constitution of the NDSC/NDACC and a number of spectrometers are now operational in several of its more than 70 remote-sensing stations covering all latitudinal bands (Boyd et al., 2007; Connor et al., 2007; Hafele et al., 2009; Nedoluha et al., 2011).

Although initially polar ozone research was mainly focused on the Antarctic (where the winter/spring ozone loss between 14 and 20 km is regularly close to 100%), in the past few years the attention has shifted towards similar but less understood mechanisms that take place in the Arctic. The main processes leading to ozone reduction are the same over the two poles. Pronounced differences in stratospheric dynamics between the two hemispheres lead, however, to larger interannual variability in the stratospheric temperatures and in the vortex stability over the Arctic with respect to what occurs over the Antarctic (e.g., Harris et al., 2010). We lack a complete understanding of the mechanisms driving this variability and of potential effects that increasing greenhouse gases may have on these processes (Manney et al., 2011). Present day Chemistry Climate Models (CCMs) underestimate the observed frequency of cold Arctic winters (WMO, 2011) and do not capture the long-term trend of the coldest winters becoming colder (Rex et al., 2006). A cooling of the polar lower stratosphere is expected to increase the occurrence and the duration of PSCs, especially in the Arctic, where observed temperatures are frequently close to the PSC formation threshold. Therefore, this general warm bias in CCMs results in the Arctic may lead to a significant underestimation of the chemical ozone loss in the Northern Hemisphere (WMO, 2011). Improving our knowledge and our predictive capabilities for the evolution of the Arctic stratosphere is one of the main atmospheric challenges of the next decades. Comprehensive long-term stratospheric data records, such as those provided by the instruments deployed in the NDACC Arctic stations (Palm et al., 2010; Hoffman et al., 2011), are a prerequisite to reach this goal.

In order to address these needs, in January 2009 the GBMS was installed at the NDACC Arctic station located at Thule (76.5° N, 68.8° W), Greenland, with the purpose of establishing a long-term observation site. Since then, four winter campaigns have been carried out during the period January–March 2009–2012 (Di Biagio et al., 2010; Muscari et al., 2012), and regular winter campaigns are planned for the future.

In the past, GBMS O<sub>3</sub> and HNO<sub>3</sub> spectra were deconvolved using a Chahine–Twomey (C–T) (Twomey et al., 1977) and an iterative constrained Matrix Inversion (MI) technique (Twomey, 1977), respectively. More recently, the GBMS retrieval algorithm has been updated to an Optimal Estimation method in order to conform to the standard of the NDACC microwave group, and to easily provide retrievals with a set of Averaging Kernels that grants more straightforward comparisons with other datasets (Fiorucci et al., 2011). Comparing ground-based measurements with satellite

observations is particularly important because, when well-validated, the ground-based data may be used to fill gaps in temporal coverage of satellite datasets. Such a gap is likely to occur in this decade, when most of the satellite missions that in the past decade have provided an accurate and global picture of the stratosphere are not expected to be replaced by follow-up missions. In this study, we present GBMS stratospheric O<sub>3</sub> and HNO<sub>3</sub> measurements obtained during the last two (for O<sub>3</sub>) or three (for HNO<sub>3</sub>) winters at Thule, illustrating briefly the main characteristic of the observing technique and the adaptation of the Optimal Estimation method to GBMS spectra. Furthermore, the accuracy of the presented data is assessed through comparisons with correlative satellite datasets from the Aura MLS experiment.

## 2 GBMS observing technique

The GBMS is a heterodyne spectrometer that measures O<sub>3</sub> and other stratospheric trace gases (such as HNO<sub>3</sub>, N<sub>2</sub>O and CO) relevant to ozone chemistry and transport in the polar regions by observing rotational transition lines emitted from these constituents between 230 and 280 GHz. Its initial prototype was designed and built at the State University of New York at Stony Brook (de Zafra, 1995) at the end of the 1980s, when increasing interest in polar ozone depletion processes developed in the atmospheric scientific community. In its present form it consists of a high sensitivity heterodyne receiver employing a cryogenically cooled SIS (Superconductor-Insulator-Superconductor) double sideband mixer with an intermediate frequency (IF) of 1.4 GHz. The two superimposed sidebands are assumed to have equal gain over the whole 230–280 GHz frequency range. This assumption originates from comparing the relative intensity of three ozone lines (at 276.9, 279.5, and 279.9 GHz) observed simultaneously by placing two lines in the upper sideband and one in the lower sideband. The front end is followed by two Acousto-Optical Spectrometers, the so-called “wide-band” spectrometer with a bandpass of 600 MHz and a resolution of 1.176 MHz, and the “narrow-band” spectrometer with a spectral window of 50 MHz and a resolution of ~ 65 kHz. The strong dependence of the line broadening on the atmospheric pressure allows for the retrieval of mixing ratio vertical profiles of the observed species, using deconvolution algorithms. The overall spectral pass band and resolution of the spectrometer used are therefore key elements to determine the altitude range over which trace gas concentrations can be measured. In particular, vertical profiles of the observed trace gases can be retrieved between ~ 15 and ~ 50 km and between ~ 35 and ~ 80 km using the GBMS wide-band and narrow-band spectrometers, respectively (Muscari et al., 2002, 2007).

The GBMS observational geometry relies on the beam switching technique first described by Parrish et al. (1988) and widely employed in millimeter-wave spectroscopy. A detailed discussion of the GBMS observing technique and involved equations can be found in de Zafra (1995) and Fiorucci et al. (2008).

GBMS O<sub>3</sub> measurements discussed in this work are obtained by observing the pure rotational transition line at 264.925 GHz (Fig. 1a). The observed HNO<sub>3</sub> spectrum is more complex and characterized by a number of superimposed, relatively weak rotational lines centered at 269.240 GHz, appearing as a single broad unresolved feature in the spectrometer pass band due to pressure broadening (Fig. 2a). An Ozone line centered outside the GBMS pass band, at 267.266 GHz, shows its signature as a background curvature superimposed to the HNO<sub>3</sub> spectra. GBMS spectra are initially saved in 15-min integration time bins but ultimately averaged together in 1–2 h (for O<sub>3</sub>) or 3–6 h (for the weaker HNO<sub>3</sub> lines) bins to improve the signal-to-noise ratio (S/N).

Since this work is focused on stratospheric O<sub>3</sub> and HNO<sub>3</sub>, only wide-band spectral data will be discussed. Upper stratospheric/mesospheric O<sub>3</sub> observations obtained from the GBMS narrow-band spectrometer have already been presented by Muscari et al. (2012).

### 3 GBMS dataset

Out of the four winter campaigns carried out at Thule during the first three months (January–March) of 2009, 2010, 2011, and 2012, the O<sub>3</sub> and HNO<sub>3</sub> ground-based observations presented in this work have been obtained only during the last two (for O<sub>3</sub>) or three (for HNO<sub>3</sub>) campaigns. During all the campaigns, measurements have been performed mostly on a daily basis, except in cases of poor weather conditions, for a total of 106 days.

In 2009, during the first measurement campaign, the observed spectra showed baseline artifacts due to a temporary malfunction of the beam balancing system. Such artifacts rendered the uncertainties in the retrieval of the weak and complex HNO<sub>3</sub> spectra exceedingly high, and these data were therefore discarded for the comparison with MLS data. Baseline issues do not affect any other GBMS spectra and are unique to the 2009 campaign. Starting in January 2011, the O<sub>3</sub> line observed by the GBMS was changed from the one at 276.923 GHz to the emission at 264.925 GHz, due to better sensitivity of the GBMS in the latter frequency range. Observations of the two transition lines yield O<sub>3</sub> data that are consistent overall. However, due to the large variability of stratospheric O<sub>3</sub> during each Arctic winter and from one winter to the next, we resolved to employ only the 2011 and 2012 O<sub>3</sub> data obtained with better sensitivity at 264.925 GHz for the intercomparison with Aura MLS. This is the emission

line that the GBMS will continue to observe in future Arctic campaigns.

In order to retrieve mixing ratio vertical profiles from GBMS spectra, an Optimal Estimation (OE) algorithm is used. A detailed description of the OE algorithm is given by Rodgers (1976, 2000), while the adaptation of the general theory to GBMS measurements has been extensively presented in Fiorucci et al. (2011) and Muscari et al. (2012). Here we briefly illustrate only those aspects of the GBMS inversion technique necessary to better characterize the retrieved profiles presented in this work.

The OE method combines information coming from the a priori profile ( $x_a$ ) and from the measurements ( $y$ ), weighting their contributions with the respective inverse covariances ( $S_\varepsilon^{-1}$  and  $S_a^{-1}$ ). The retrieval solution is given by:

$$x_r = \frac{S_a^{-1}x_a + K^T S_\varepsilon^{-1}y}{S_a^{-1} + K^T S_\varepsilon^{-1}K} \quad (1)$$

where the weighting functions  $K$  describe the sensitivity of the spectrum to changes in the true atmospheric profile (hereinafter referred to as “the atmosphere”). The relative weight of the a priori profile and of the measured spectrum depends on the physical (forward) model included in  $K$ , as well as on the error covariances  $S_\varepsilon$  and  $S_a$  (in particular on the ratio  $S_\varepsilon$  to  $S_a$  rather than on their absolute values). In fact, assigning a small uncertainty to the a priori profile constrains the retrieved profile to the a priori information, while if the adopted  $\sigma_a^2$  values (diagonal elements of  $S_a$ ) are too large, solutions rely mostly on the spectral measurement but may have the tendency to oscillate.

Here we take a priori information for both species from the Aura MLS data sets, considered to be accurately validated estimates for the quantities under investigation. All of the MLS O<sub>3</sub> and HNO<sub>3</sub> profiles measured over the GBMS observing periods (approximately from mid-January to mid-March 2010, 2011, and 2012 for HNO<sub>3</sub>, 2011 and 2012 for O<sub>3</sub>) within 1° latitude and 8° longitude from Thule are averaged together to give one O<sub>3</sub> and one HNO<sub>3</sub> profile. Using a single a priori for each of the two datasets ensures that the interannual differences as well as the seasonal evolution observed in the GBMS datasets do not depend on the a priori. The choice of using MLS averages as a priori information for the GBMS deconvolution process might appear questionable. However, it should be noted that after convolving MLS profiles with the GBMS AVK’s and a priori profile (see Sects. 3.1 and 6 and Connor et al., 2007, Eq. 3) the differences between GBMS and MLS profiles are entirely independent of the specific a priori profile employed. Moreover, in the altitude range of interest, both O<sub>3</sub> and HNO<sub>3</sub> GBMS retrievals are strongly dependent on the measured spectra and largely independent of the a priori (see Sects. 3.1 and 3.2).

For O<sub>3</sub> retrievals we choose a priori profile variances (diagonal elements of  $S_a$ ) varying from 50 to 80 %, depending on altitude, and consider a correlation length of 5 km between

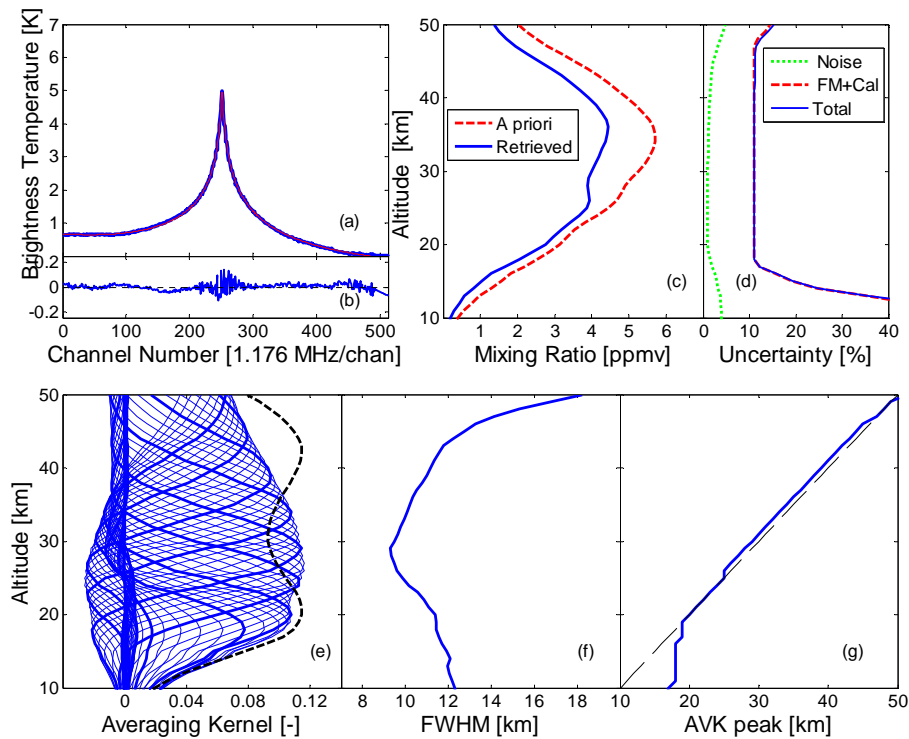


**Fig. 1.** Retrieval results for the GBMS O<sub>3</sub> spectrum recorded at Thule on 20 February 2011. **(a)** Spectrum observed by the GBMS (blue line) and forward model-generated from the OE retrieved profile (superimposed, in red). The O<sub>3</sub> line is located at 264.926 GHz and the spectral window is 600 MHz wide. **(b)** Spectral residuals (measured spectrum minus forward-generated spectrum). **(c)** O<sub>3</sub> profile retrieved from the measured spectrum displayed in **(a)** (blue line) together with the a priori profile (red dashed line). **(d)** Total 1 $\sigma$  uncertainty on the retrieved profile (in blue) with its different contributions: the red dashed line indicates uncertainty due to calibration, data scaling procedures and forward model parameters, the green dotted line represents the uncertainty due to spectral noise. **(e)** GBMS Averaging Kernels (blue lines) and total sensitivity, as defined in the text, divided by 10 (dashed black line). Thicker blue lines are AVKs calculated at each 5 km altitude. **(f)** Vertical resolution of retrieved profile estimated as the FWHM of the AVKs. **(g)** Altitude of the peak of the AVKs versus their nominal altitude (blue line). The one-to-one line is also shown (dashed black).

gas concentrations at different altitudes.  $S_a$  is held constant for the analysis of the entire dataset. We assume the covariance matrix of the measurement vectors to be diagonal, with all the diagonal elements  $\sigma_\epsilon^2$  equal, and use these diagonal elements as adjustable parameters for optimizing the retrieval sensitivity. In particular, we choose the smallest value (corresponding to the highest resolution) producing solution profiles which do not display nonphysical oscillations. The  $\sigma_\epsilon^2$  eventually adopted is also held constant throughout the analysis and is of the same order of magnitude as the O<sub>3</sub> spectral residuals (i.e., the differences between the measured spectra and those generated from the retrieved profiles using the forward model).

HNO<sub>3</sub> spectra are characterized by many HNO<sub>3</sub> lines blended together by pressure broadening and contaminated by a weak ozone line and by the tail of an intense O<sub>3</sub> emission outside the pass band. Thus, they are more difficult to retrieve and are inverted using a two-step process. At the first step, the HNO<sub>3</sub> and O<sub>3</sub> signatures appearing in the GBMS pass band are simultaneously retrieved with  $S_a$  and  $S_\epsilon$  matrices

chosen according to the same criteria adopted for the O<sub>3</sub> retrieval. In order to extract more information from the HNO<sub>3</sub> emission, the O<sub>3</sub> background obtained at the first step is then subtracted from the overall observed spectral signal. The resulting HNO<sub>3</sub> only spectrum is ultimately inverted again with a larger weight placed on the spectral measurement (smaller  $\sigma_\epsilon^2$  values) with respect to the a priori profile. This second phase, aimed at maximizing the sensitivity and vertical resolution of the HNO<sub>3</sub> retrieval, cannot be carried out in the presence of the O<sub>3</sub> background signal. The HNO<sub>3</sub> only spectrum is inverted using the same a priori profile and  $S_a$  matrix as in the first inversion, but with  $\sigma_\epsilon^2$  values which are different from spectrum to spectrum and are assigned to be proportional to the spectral noise (estimated using the RMS of the spectral residual measured at the first step of the inversion process).

Spectroscopic parameters necessary to calculate the absorption coefficients for a given molecular transition are taken from the Jet Propulsion Laboratory (JPL) spectral catalog (available at <http://spec.jpl.nasa.gov>) (Pickett et al.,

1998) (lines intensities) and from the HITRAN2008 database (Rothman et al., 2009) (pressure broadening and temperature dependence coefficients). Atmospheric pressure and temperature profiles used for the analysis in this study are obtained from MLS observations for the specific dates and location.

### 3.1 O<sub>3</sub> retrievals

In Fig. 1, the retrieval results for the GBMS O<sub>3</sub> spectrum recorded at Thule on 20 February 2011 are presented. Panel a shows the spectrum observed by GBMS and, superimposed, the spectrum calculated from the corresponding OE retrieved profile (displayed in panel c together with the a priori profile); the difference between the two spectra (spectral residual) is drawn in panel b. Panel e depicts the Averaging Kernel functions (AVKs), which are the rows of the Averaging Kernel matrix, defined in the OE method as  $\mathbf{A} = \partial x_r / \partial x$  (e.g., Rodgers, 2000). Each AVK represents the sensitivity of the retrieval ( $x_r$ ) at a given altitude to variations in the atmosphere ( $x$ ) at all altitudes. When they are well-peaked functions, centered at their nominal altitude, a perturbation in the atmosphere is attributed to the correct altitude in the retrieved profile. Furthermore, the area enclosed under each kernel is an indication of the total sensitivity of the retrieved profile at that altitude to atmospheric variations. Sensitivity values close to 1 indicate that the major contribution to the solution comes from the spectral measurement rather than from the a priori. In the altitude range where both these conditions are satisfied (i.e., there is correspondence between the AVKs' nominal and peak altitudes, and the sensitivity is close to 1), the retrieval responds satisfactorily to changes in the atmosphere, and the AVKs' full width at half maximum (FWHM) can be used as a rough measure of the local vertical resolution of the obtained mixing ratio vertical profile. The sensitivity curve derived from the AVKs is displayed in panel e (superimposed to the AVKs), while their FWHM's are shown in panel f. Differences between the nominal height of each AVK and the actual height where it peaks are shown in panel g.

Results shown in panels e, f and g suggest that our retrieval has good sensitivity (> 80 %) in the vertical range ~ 17–50 km, where the difference between the nominal and the peak height of the AVKs does not exceed 3 km and the vertical resolution is between ~ 9 and 18 km (but remains under 12 km up to 44 km). This is the vertical range over which GBMS O<sub>3</sub> profiles may be used for scientific purposes. Finally, panel d shows the total error on the retrieved profile with its different contributions. Errors on GBMS profiles are mainly due to instrument calibration and data scaling procedures (~ 8 %), and to parameters used in the forward model calculation (7 %) (Parrish et al., 1988; Cheng et al., 1996). These two contributions add up (in quadrature) to an overall  $\pm 1\sigma$  of ~ 11 % (red dashed line). The uncertainties related to the calibration and data scaling (e.g., errors in receiver temperature and atmospheric opacity) can be both systematic

and random, also depending on the time periods considered and local weather conditions (most likely systematic during short periods of very stable weather and random over long periods comprising different field campaigns). Similarly, we consider spectroscopic parameters as a source of systematic error, whereas pressure and temperature vertical profiles cause mostly random errors. As a distinction between fixed and variable errors is not always possible in this context, we conservatively consider all the above-mentioned uncertainties to be systematic. The error due to measurement noise (green dashed dotted line) is determined following the OE procedure presented in Connor et al. (2006) and gives a small contribution to the overall uncertainty (< 5 % at all altitudes).

One additional error source (not included in the plot of Fig. 1d) is the limited vertical resolution of the observing technique. This leads to solution profiles that are a smoothed version of the atmosphere and that do not exhibit the fine vertical structure of the actual profiles. Many authors in the OE literature suggest that this error, called “smoothing error”, should be estimated only if accurate knowledge of the variability of the atmospheric fine structure is available (Connor et al., 1995; Rodgers, 2000). We follow this prescription and do not include the smoothing error in our error estimate. Additionally, this resolution error can be completely removed from comparisons with datasets having a higher vertical resolution (e.g., the Aura MLS data in this work) by “convolving” the higher resolution profiles with the AVKs of the lower resolution data (GBMS):

$$x_{\text{conv}} = x_a + \mathbf{A}_{\text{GBMS}}(x_{\text{MLS}} - x_a) \quad (2)$$

The total uncertainty of the retrieved profiles, determined by adding in quadrature the above mentioned contributions, generally amounts to 11 % (blue line), with a minimum absolute error of 0.2 ppmv and small differences depending on observing conditions. The reader is directed to Fiorucci et al. (2011) for more details on the error analysis.

### 3.2 HNO<sub>3</sub> retrievals

An illustrative inversion of the HNO<sub>3</sub> spectrum (after the subtraction of the O<sub>3</sub> background line) is presented in Fig. 2. Similarly to Fig. 1, the measured and forward-model generated spectra are presented in panel a, their difference in panel b, the a priori and retrieved mixing ratio profiles in panel c and the uncertainties on the retrieved profiles in panel d. Panels e and f depict the AVKs with their sensitivity curve, and the FWHM of the kernels, respectively. Differences between the AVKs' nominal and peak altitude are shown in panel g. Fig. 2 (panels e and g) shows that the AVKs are well peaked and centered close to their correct altitude level in the vertical range 17–45 km, with their sensitivity close to 1. The vertical resolution varies from 9 to 14 km in this vertical range (panel f), which is the one recommended for scientific use of the GBMS HNO<sub>3</sub> dataset.

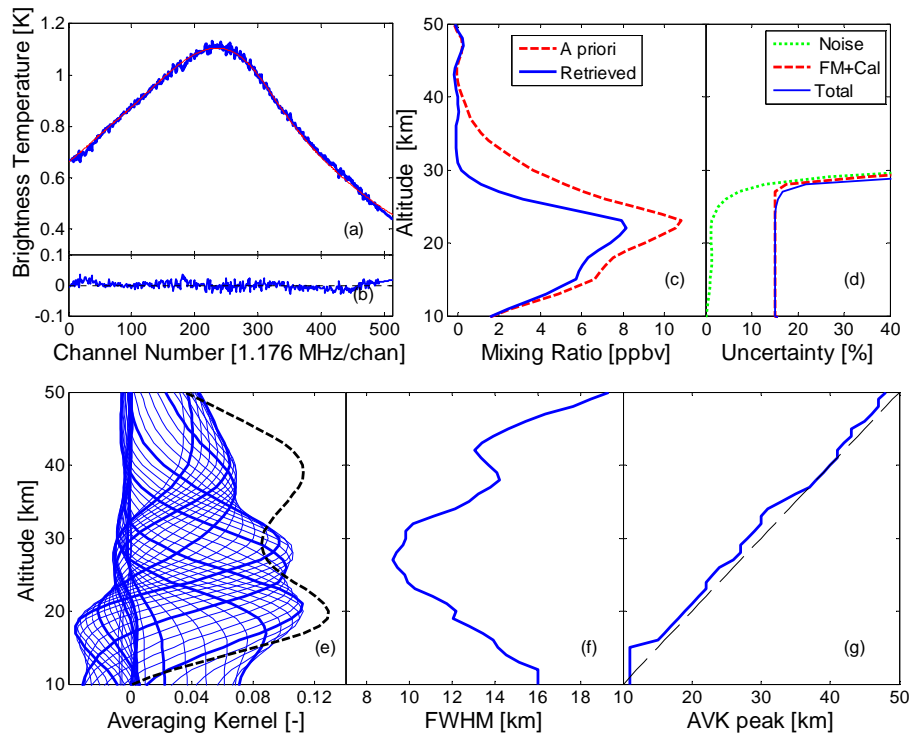


**Fig. 2.** As in Fig. 1, but for GBMS HNO<sub>3</sub> retrievals. The 600 MHz spectral pass band where the HNO<sub>3</sub> lines are located ranges from 268.911 to 269.511 GHz.

The total uncertainty has been assessed following the same criteria used for O<sub>3</sub> and is given by the larger of 15 % or 0.2 ppbv (see also Fiorucci et al., 2011), with the main contribution given by uncertainties due to calibration and to parameters used in the forward model calculation. It is worth stressing that the relative uncertainty becomes very large above ~28 km due to very low HNO<sub>3</sub> concentrations, whereas the absolute error remains as low as 0.2 ppbv throughout the vertical range.

#### 4 Correlative datasets

The Microwave Limb Sounder is one of four instruments aboard Aura, the latest NASA Earth Observing System satellite, launched on 15 July 2004 into a near-polar, sun-synchronous orbit (Waters et al., 2006; Schoeberl et al., 2006). Aura MLS observes several atmospheric constituents by measuring millimeter and submillimeter wavelength thermal emission from Earth's limb using five broad spectral bands between 118 GHz and 2.5 THz. The Aura orbit and MLS viewing geometry (viewing forward along the flight direction and vertically scanning the limb) lead to data coverage from 82° S to 82° N latitude on every orbit, with ~13 orbits per day (Santee et al., 2007).

MLS mixing ratio vertical profiles are retrieved using an algorithm based on the Optimal Estimation method (Livesey

et al., 2006). All the data presented in this comparison are processed with the version 3.3 (v3.3) algorithms, the third “public release” of MLS data. Main changes, improvements, and issues with v3.3 data are discussed in the v3.3 MLS data quality document (Livesey et al., 2011; <http://mls.jpl.nasa.gov/data/datadocs.php>).

#### 4.1 Aura MLS O<sub>3</sub> observations

The MLS O<sub>3</sub> standard product for version 3.3 is taken from the 240 GHz retrieval and is recommended for scientific use over the range 261 to 0.02 hPa. Based on the FWHM of the Averaging Kernels, the vertical resolution is ~2.5 km in the uppermost troposphere and stratosphere, whereas the horizontal (along-track) resolution varies from 300 to 450 km. The cross-track resolution, determined by the 240 GHz radiometer field of view, is fixed at 6 km. The single-profile precision ranges between 0.02 and 0.2 ppmv in the same vertical range (i.e., uppermost troposphere and stratosphere). Ozone profiles from v3.3 are very similar to v2.2 profiles in the stratosphere and above, so the stratospheric results reported in v2.2 validation papers (Froidevaux et al., 2008; Jiang et al., 2007; Livesey et al., 2008) generally hold for the v3.3 product as well. All these studies show generally good agreement (within 5–10 %) between MLS data and satellite, balloon, aircraft, and ground-based measurements. More detailed information on the useful vertical range, resolution and



precision of the v3.3 O<sub>3</sub> data, as well as results from comparisons with other datasets, can be found in Sect. 3.17 of Livesey et al. (2011).

#### 4.2 Aura MLS HNO<sub>3</sub> observations

The HNO<sub>3</sub> product is derived from the 240 GHz radiometer for atmospheric pressures equal to or greater than 22 hPa and from the 190 GHz radiometer at higher altitudes. MLS HNO<sub>3</sub> retrievals have been greatly improved in v3.3. Comparisons with correlative satellite and ground-based datasets suggest that the negative bias ( $\sim 10$ – $30$  %) observed throughout most of the stratosphere in the v2.2 HNO<sub>3</sub> profiles has been largely removed in v3.3. The latter profiles are recommended for scientific use over the range 215–1.5 hPa, with a single-profile precision, empirically estimated, of  $\sim 0.6$ – $0.7$  ppbv throughout the range from 100 to 3.2 hPa, below and above which it increases sharply. The effects of systematic uncertainties on v3.3 measurements have not been completely assessed but are expected to be very similar to those estimated for v2.2 (measurement biases varying with altitude between  $\sim 0.5$  and  $\pm 2$  ppbv and multiplicative errors of  $\pm 5$ – $15$  % throughout the stratosphere). The vertical resolution varies between 3 and 5 km, depending on altitude. The along-track horizontal resolution is 450–500 km over most of the vertical range, whereas the cross-track resolution, set by the width of the field-of-view of the 190 GHz and 240 GHz radiometers, is  $\sim 10$  km (Sect. 3.11 Livesey et al., 2011).

#### 5 Comparison criteria

Being in near-polar orbit, Aura MLS provides each day closely spaced observations near high latitude sites. This intercomparison work can therefore count on a satisfactory number of daily MLS observations near Thule to be matched to GBMS measurements. The Arctic stratosphere during winter/spring periods is often characterized, however, by particularly patchy distributions of chemical compounds. This condition could spoil comparison results if stringent coincidence criteria (both spatial and temporal) between the two datasets were not implemented. Dynamical, chemical and microphysical processes, including rapid ClO activation (and consequent O<sub>3</sub> depletion) and HNO<sub>3</sub> sequestration in PSCs, can induce strong spatial and temporal concentration gradients in both considered species. In order to overcome these issues, for each GBMS measurement we first select MLS observations within a box of  $\pm 1^\circ$  latitude and  $\pm 8^\circ$  longitude from the GBMS observing site. Then, among the selected MLS profiles, we choose the closest in time to the GBMS measurement, discarding those that are more than 6 h away from the limits of the GBMS integration interval. Using the above mentioned requirements, we obtain a total of 43 coincidences between GBMS and MLS for the HNO<sub>3</sub> comparison (7 in 2010, 19 in 2011 and 17 in 2012) and 54 for the

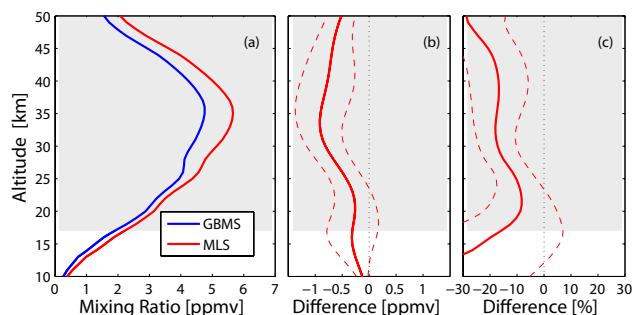


**Fig. 3.** Comparison of GBMS O<sub>3</sub> profiles with co-located Aura MLS observations obtained during the two winters 2011 and 2012 (54 coincidences). **(a)** GBMS (blue) and MLS convolved (red) mean profiles. **(b)** Mean absolute difference between GBMS and MLS convolved profiles. Dashed lines represent the standard deviation of the mean difference. **(c)** As in **(b)**, but indicating percent differences (calculated by dividing the mean difference (GBMS – MLS) by the mean (GBMS + MLS)/2). The vertical range where the retrieval has a good sensitivity ( $> 80$  %) is highlighted with a grey background.

O<sub>3</sub> (27 both in 2011 and 2012). Sensitivity tests have been carried out to make sure that the comparison results do not change significantly if more stringent spatial and temporal selection criteria are employed. We first examine the sensitivity of the results to the box size, testing a reduced box of  $\pm 0.5^\circ$  latitude and  $\pm 4^\circ$  longitude. Then the time criterion is investigated, selecting MLS data within  $\pm 3$  h from GBMS observations. These tests show that the stricter constraints on both spatial and temporal matching criteria reduce the number of coincidences without significantly modifying the comparison results.

Two additional criteria are used to select air masses which have experienced similar dynamical and chemical conditions: the Potential Vorticity (PV), useful to differentiate inner vortex from extra vortex air, and the temperature, which is a key parameter in chemical processes within the polar vortex. In order to include these criteria in our selection procedure, we have examined daily maps with analysis of PV and temperature values at 550 K provided by the Danish Meteorological Institute. PV values between 70 and  $80 \times 10^{-6} \text{ K m}^2 \text{ s}^{-1} \text{ kg}^{-1}$  are used to identify the vortex edge, while 192 K is considered the formation temperature threshold for type I PSCs at this altitude (assuming a 10 ppbv concentration of HNO<sub>3</sub> and 5 ppmv of H<sub>2</sub>O) (Larsen et al., 1997, 2000).

By using these proxies we eliminate from the comparison those profile pairs in which GBMS and MLS sampled air masses on opposite sides of the vortex edge or matches when either or both instruments looked inside the area of possible formation of PSCs. The latter selection process does not affect the results, and therefore in order to increase the statistical significance of the intercomparison we did not implement it in the end. Finally, MLS data that did not pass all the

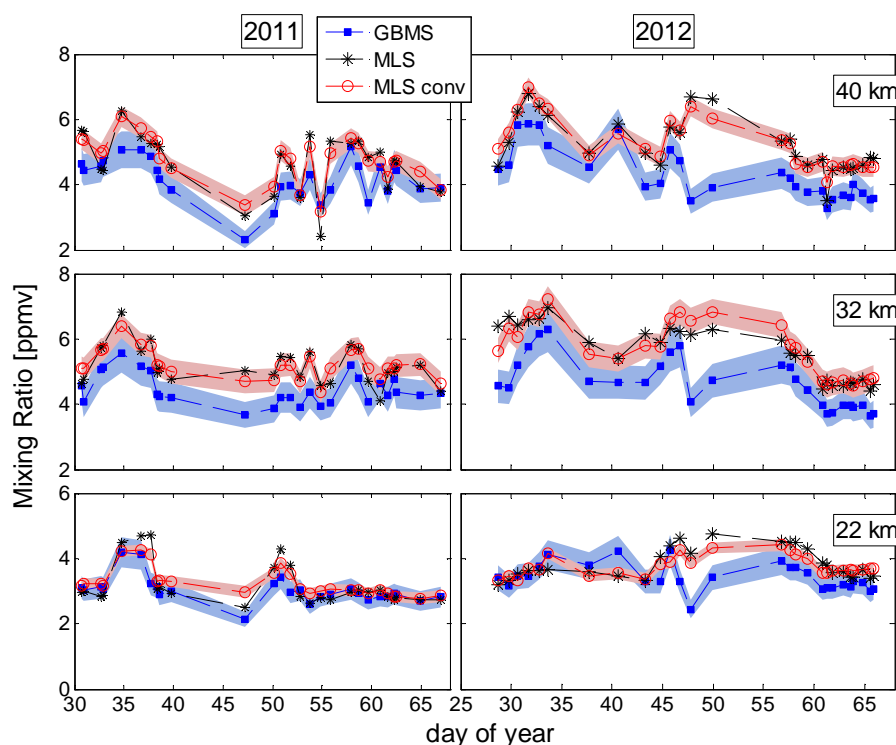


**Fig. 4.** Timeseries of GBMS (blue squares), Aura MLS (black stars) and convolved Aura MLS (open red circles) O<sub>3</sub> data for 2011 (left panels) and 2012 (right panels) at three altitude levels: 22 km, 32 km and 40 km. The blue shaded area depicts the GBMS uncertainty, calculated as described in Sect. 3.1 and shown in Fig. 1. Uncertainties on the convolved MLS data (red shaded area) include both systematic and random errors.

v3.3 quality control criteria have been left out of the comparison. The same fate occurred to GBMS measurements for which the observed spectrum has been poorly fitted by the retrieval algorithm (RMS of spectral residual > 0.05 K). Due to the different vertical resolutions of the instruments (see Sects. 3.1, 3.2, 4.1 and 4.2), before comparing the selected pairs of measurements the higher resolution MLS profiles are interpolated to the GBMS retrieval grid and convolved using the appropriate GBMS AVKs and a priori profile.

## 6 Results

In Figs. 3, 4 and 5 (6, 7 and 8) we present results of comparisons of stratospheric O<sub>3</sub> (HNO<sub>3</sub>) from Aura MLS v3.3 and GBMS. Figure 3a shows MLS and GBMS O<sub>3</sub> mean profiles obtained by averaging together 54 observations from the years 2011 and 2012. Panels b and c of Fig. 3 illustrate absolute and percent differences, respectively, between the convolved MLS and GBMS O<sub>3</sub> profiles, with dashed lines indicating  $\pm 1\sigma$  of the mean difference. The two datasets display good agreement up to 26 km, with the GBMS being lower than the convolved MLS by less than 0.5 ppmv ( $\sim 10\%$ ). Above 26 km the agreement

worsens with increasing altitude, with a maximum difference of  $\sim 0.9$  ppmv ( $\sim 18\%$ ) near the profile peak.

In order to investigate the correlation between MLS and GBMS O<sub>3</sub> data presented in Fig. 3, Fig. 4 shows time series of all the selected MLS-GBMS pairs of values at three altitude levels (22, 32 and 40 km). As mentioned in Sect. 5, to account for the different vertical resolution between the ground- and the satellite-based data, each MLS profile has been convolved with the respective GBMS set of AVKs before the comparison. For the purpose of illustrating the effect of the convolution on MLS O<sub>3</sub> profiles, in Fig. 4 we show both the original (black stars) and the convolved (red open circles) values. The red and blue shaded areas represent the uncertainties on MLS (convolved) and GBMS O<sub>3</sub> data, respectively. The indicated MLS uncertainty includes both systematic and random errors, whereas the GBMS error bars are calculated as described in Sect. 3.1.

Figure 4 shows that GBMS O<sub>3</sub> mixing ratio values track MLS daily variations reasonably well, and confirms that the former dataset has a negative bias with respect to the satellite observations. This bias is essentially consistent in both years and depends on the altitude level. In order to evaluate the capability of GBMS measurements to follow seasonal and interannual O<sub>3</sub> variations (e.g., to quantify the spring-time ozone loss), a scatterplot of MLS vs. GBMS O<sub>3</sub> partial



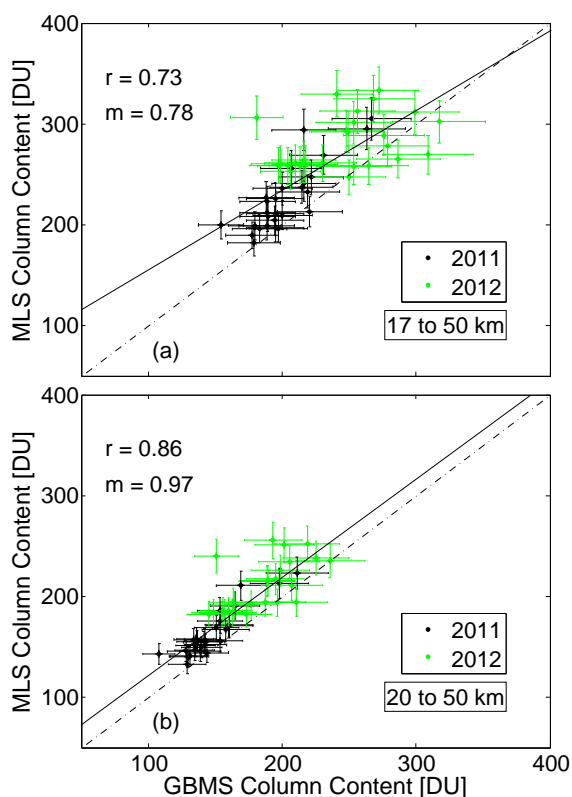


**Fig. 5.** (a) Scatterplot of Aura MLS against GBMS O<sub>3</sub> column content integrated between 17 and 50 km. Different colors denote different years: 2011 (black) and 2012 (green). Vertical and horizontal error bars represent MLS and GBMS uncertainties, respectively. Linear fit to the data points is displayed with a solid line, and the 1 : 1 bisector is represented with dash-dotted lines. The correlation coefficient ( $r$ ) and the slope of the linear fit ( $m$ ) are also reported. (b) As in (a), but integrating between 20 and 50 km.

column contents integrated between 17 and 50 km (the altitude range over which GBMS profiles are considered reliable) is displayed in Fig. 5a. A correlation coefficient of 0.73 and a slope of 0.78 for the linear fit to the data indicate a generally good correlation between the two datasets, with the GBMS O<sub>3</sub> values having a larger variability with respect to MLS data. If the same plot is drawn for column contents between 20 and 50 km (Fig. 5b), thus excluding the bottom 3 km of the altitude range considered scientifically meaningful, then the correlation improves to a coefficient of 0.86 and a slope of 0.97. This suggests that the O<sub>3</sub> partial column variations detected by the GBMS agree well with those measured by the Aura MLS, particularly from 20 km upwards.

Figures 6, 7 and 8 are analogous to Figs. 3, 4 and 5, but concern HNO<sub>3</sub> measurements. MLS and GBMS HNO<sub>3</sub> peak absolute values (Fig. 6) agree fairly well. Figure 6b and c show a positive bias of GBMS versus MLS measurements, reaching a maximum of  $\sim 1$  ppbv (10 %) near the profile peak. This bias decreases above the profile peak and becomes negative above 26 km. Above 30 km,

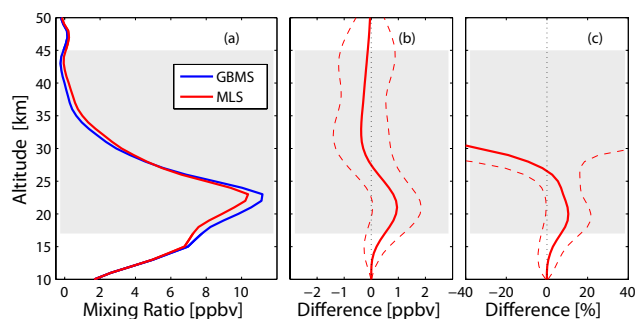


**Fig. 6.** Same as in Fig. 3, but for the HNO<sub>3</sub> intercomparison. A total of 43 coincidences was found.

as the HNO<sub>3</sub> concentrations decrease with altitude to very small values, the relative difference between GBMS and MLS (i.e.,  $2 \cdot (\text{GBMS} - \text{MLS}) / (\text{GBMS} + \text{MLS})$ ) becomes very large and loses significance. The mean difference in absolute values between the two datasets remains within one standard deviation over the whole vertical range (Fig. 6b).

Figure 7 shows that GBMS HNO<sub>3</sub> measurements are generally well correlated with both the original and the convolved MLS observations during the three years considered and at all altitudes. In Fig. 8, the correlation coefficient (0.92) and the slope of the linear fit (0.95) indicate that the partial columns of the two datasets (integrated over the GBMS vertical range suggested for scientific use) are well correlated and therefore their variations are in close agreement. In contrast to the O<sub>3</sub> case, for HNO<sub>3</sub> the correlation parameters do not change significantly when the altitude interval over which the column contents are calculated is changed. This discrepancy between the two sets of comparisons is under investigation.

GBMS HNO<sub>3</sub> observations from mid-latitudes have been previously compared to Aura MLS measurements. In particular, GBMS measurements carried out at the Alpine site of Testa Grigia (45.9° N, 7.7° E, elev. 3500 m) in 2005 were found to be  $\sim 3$  ppbv (20–30 %) higher than satellite data near the profile peak (Santee et al., 2007). However, both the GBMS and the MLS retrieval algorithms have been revised since then. Fiorucci et al. (2011) compared GBMS profiles retrieved applying the “old” and the “new” techniques to the same set of spectra, finding that the former set of profiles (v1) were systematically larger near the peak by up to 2 ppbv with respect to v2 profiles. On the other hand, as seen in Sect. 4.2, MLS HNO<sub>3</sub> values have increased from v2.2 to v3.3 by about 20–30 % throughout most of the stratosphere (Livesey et al., 2011). A GBMS versus MLS HNO<sub>3</sub> intercomparison plot obtained using the most recent algorithms applied to mid-latitude observations during winters 2004/2005, 2005/2006, and 2006/2007 is shown in Livesey et al. (2011) (on page 88). The above-mentioned results suggest that, on average, GBMS and MLS HNO<sub>3</sub> data from the mid-latitudes compare to one another similarly to what is shown in this work for the high latitudes, with the GBMS displaying a small but non-negligible positive bias at the HNO<sub>3</sub> mixing ratio peak.

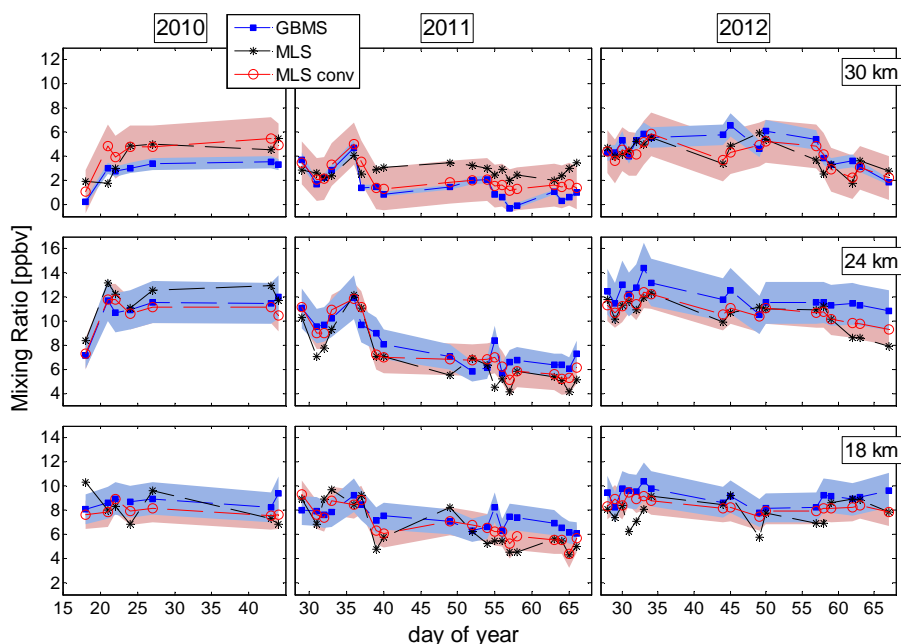


Fig. 7. Same as in Fig. 4, but for HNO<sub>3</sub> data. HNO<sub>3</sub> values are displayed at 18, 24 and 30 km altitude.

## 7 Summary and conclusions

In this study, we present O<sub>3</sub> and HNO<sub>3</sub> GBMS measurements obtained at the NDACC station in Thule, Greenland, during the last two (for O<sub>3</sub>) or three (for HNO<sub>3</sub>) winters. We give a characterization of the retrieved profiles (altitude range of sensitivity, vertical resolution, total uncertainty) and assess their accuracy by comparing them with the well-validated Aura MLS observations. This is relevant to the scientific community since the GBMS O<sub>3</sub> and HNO<sub>3</sub> retrievals are publicly available on the NDACC database and may be used in future studies on the Arctic winter stratosphere. Moreover, in the event that operational satellite missions would be reduced in the future, it is useful to assess to what extent ground-based microwave instruments can help to fill the consequent gaps in atmospheric data.

In this work it is shown that GBMS O<sub>3</sub> profiles can be considered for scientific use between  $\sim 17$  and  $\sim 50$  km, with an overall  $1\sigma$  uncertainty that amounts to the larger of  $\sim 11\%$  or 0.2 ppmv and a vertical resolution between about 9 and 18 km. Similarly, HNO<sub>3</sub> measurements have good sensitivity over the range  $\sim 17$ –45 km and a vertical resolution encompassed between about 9 and 14 km in this altitude range. The  $1\sigma$  uncertainty is given by the larger of 15% or 0.2 ppbv.

Results presented in Sect. 6 illustrate that the GBMS O<sub>3</sub> mean profile displays a negative bias with respect to MLS throughout the considered altitude range. However, the difference between the two averaged profiles remains below 0.5 ppmv ( $\sim 10\%$ ) in the lower stratosphere and below 0.9 ( $\sim 18\%$ ) ppmv in the mid- to upper stratosphere. Moreover, GBMS and MLS O<sub>3</sub> mixing ratio values correlate reasonably

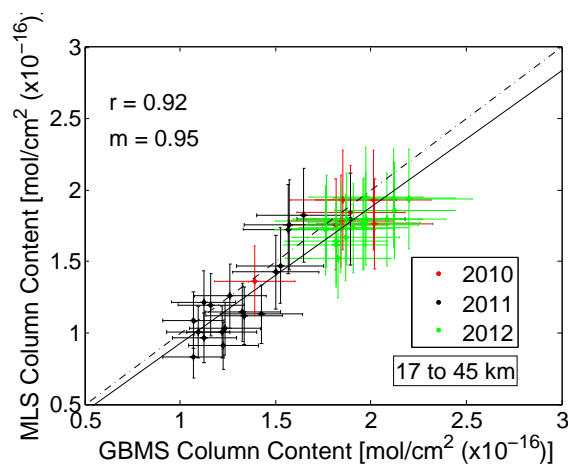


Fig. 8. Same as in Fig. 5, but for HNO<sub>3</sub> column content from 17 to 45 km altitude.

well at all altitudes, with very good results found for partial columns calculated from 20 km upwards.

The averaged GBMS HNO<sub>3</sub> profile shows values that are larger than those measured by MLS, with differences below  $\sim 10\%$  (1 ppbv at the mixing ratio peak), up to 26 km. Upwards the absolute difference decreases and becomes negative. Timeseries of GBMS and MLS HNO<sub>3</sub> values at three different altitude levels and partial column variations (from 17 km upwards) show that the ground-based and the satellite HNO<sub>3</sub> data are well correlated.

Furthermore, the overall agreement between Aura MLS and GBMS HNO<sub>3</sub> observations has significantly improved

since their previous intercomparison at mid-latitudes (Santee et al., 2007). This can be explained with the changes made in the meantime in both the GBMS and the MLS retrieval algorithms.

We showed that GBMS retrievals may be successfully used to follow seasonal (i.e., from winter to spring or from inside to outside the polar vortex) and interannual O<sub>3</sub> and HNO<sub>3</sub> variations in the Arctic winter stratosphere, as long as the estimated uncertainty and vertical resolution are taken into account. In fact, the poor vertical resolution of the GBMS HNO<sub>3</sub> profiles affects the GBMS capability of depicting correctly the removal of gas-phase HNO<sub>3</sub>, when the latter occurs over limited altitude ranges, but these data does represent a valuable asset for estimating column gas-phase HNO<sub>3</sub> removal upwards of 17 km. Similarly, GBMS O<sub>3</sub> measurements are proven capable of providing a useful quantitative estimate of the springtime ozone loss.

*Acknowledgements.* This material is based on work also supported by the National Science Foundation under grant 0936365 and by the Programma Nazionale di Ricerca in Antartide (PNRA) under grant 2009/A3.04. G. Muscari is indebted to Bob de Zafra for designing, building, and upgrading the GBMS, as well as for the economic and technical support that led to many successful GBMS field campaigns. We thank Pietro Paolo Bertagnolio, Svend Erik Ascanius, Claudia Di Biagio, and Giorgio di Sarra for their technical assistance during the GBMS field campaigns at Thule. We would also like to thank two anonymous referees and the Editor for their comments which greatly helped to improve this paper. Work at the Jet Propulsion Laboratory, California Institute of Technology, was done under contract with NASA.

Edited by: D. Feist

## References

- Boyd, I. S., Parrish, A. D., Froidevaux, L., von Clarmann, T., Kyrölä, E., Russell III, J. M., and Zawodny, J. M.: Ground-based microwave ozone radiometer measurements compared with Aura-MLS v2.2 and other instruments at two Network for Detection of Atmospheric Composition Change sites, *J. Geophys. Res.*, 112, D24S33, doi:10.1029/2007JD008720, 2007.
- Cheng, D., de Zafra, R. L., and Trimble, C.: Millimeter wave spectroscopic measurements over the South Pole, 2. An 11-month cycle of stratospheric ozone observations during 1993–1994, *J. Geophys. Res.*, 101, 6781–6793, 1996.
- Connor, B. J., Barrett, J. W., Parrish, A., Solomon, P. M., De Zafra, R. L., and Jaramillo, M.: Ozone Over McMurdo Station, Antarctica, Austral Spring 1986: Altitude Profiles for the Middle and Upper Stratosphere, *J. Geophys. Res.*, 92, 13221–13230, doi:10.1029/JD092iD11p13221, 1987.
- Connor, B. J., Parrish, A., Tsou, J. J., and McCormick, M. P.: Error analysis for the ground-based microwave ozone measurements during STOIC, *J. Geophys. Res.*, 100, 9283–9291, doi:10.1029/94JD00413, 1995.
- Connor, B. J., Mooney, T., Barrett, J., Solomon, P., Parrish, A., and Santee M.: Comparison of ClO measurements from the Aura Microwave Limb Sounder to ground-based microwave measurements at Scott Base, Antarctica, in spring 2005, *J. Geophys. Res.*, 112, D24S42, doi:10.1029/2007JD008792, 2007.
- de Zafra, R. L.: The ground-based measurements of stratospheric trace gases using quantitative millimeter wave emission spectroscopy, in *Diagnostic tools in atmospheric physics, Proceedings of the international school of physics “Enrico Fermi”, 23–54, Società italiana di fisica, Bologna, 1995.*
- de Zafra, R. L., Jaramillo, M., Parrish, A., Solomon, P. M., Connor, B., and Barrett, J.: High concentrations of chlorine monoxide at low altitudes in the Antarctic spring stratosphere: Diurnal variation, *Nature*, 328, 408–411, 1987.
- de Zafra, R. L., Chan, V., Crewell, S., Trimble, C., and Reeves, J. M.: Millimeter wave spectroscopic measurements over the South Pole: 3. The behavior of stratospheric nitric acid through polar fall, winter, and spring, *J. Geophys. Res.*, 102, 1399–1410, 1997.
- Di Biagio, C., Muscari, G., di Sarra, A., de Zafra, R. L., Eriksen, P., Fiorucci, I., and Fuà, D.: Evolution of temperature, O<sub>3</sub>, CO, and N<sub>2</sub>O profiles during the exceptional 2009 Arctic major stratospheric warming as observed by lidar and mm-wave spectroscopy at Thule (76.5° N, 68.8° W), Greenland, *J. Geophys. Res.*, 115, D24315, doi:10.1029/2010JD014070, 2010.
- Fiorucci, I., Muscari, G., Bianchi, C., Di Girolamo, P., Esposito, F., Grieco, G., Summa, D., Bianchini, G., Palchetti, L., Cacciani, M., Di Iorio, T., Pavese, G., Cimini, D., and de Zafra, R. L.: Measurements of low amounts of precipitable water vapor by millimeter wave spectroscopy: An intercomparison with radiosonde, Raman lidar, and Fourier transform infrared data, *J. Geophys. Res.*, 113, D14314, doi:10.1029/2008JD009831, 2008.
- Fiorucci, I., Muscari, G., and de Zafra, R. L.: Revising the retrieval technique of a long-term stratospheric HNO<sub>3</sub> dataset: from a constrained matrix inversion to the optimal estimation algorithm, *Ann. Geophys.*, 29, 1317–1330, doi:10.5194/angeo-29-1317-2011, 2011.
- Froidevaux, L., Jiang, Y. B., Lambert, A., Livesey, N. J., Read, W. G., Waters, J. W., Browell, E. V., Hair, J. W., Avery, M. A., McGee, T. J., Twigg, L. W., Sunmicht, G. K., Jucks, K. W., Margitan, J. J., Sen, B., Stachnik, R. A., Toon, G. C., Bernath, P. F., Boone, C. D., Walker, K. A., Filipiak, M. J., Harwood, R. S., Fuller, R. A., Manney, G. L., Schwartz, M. J., Daffer, W. H., Drouin, B. J., Cofield, R. E., Cuddy, D. T., Jarnot, R. F., Knosp, B. W., Perun, V. S., Snyder, W. V., Stek, P. C., Thurstans, R. P., and Wagner, P. A.: Validation of Aura Microwave Limb Sounder stratospheric ozone measurements, *J. Geophys. Res.*, 113, D15S20, doi:10.1029/2007JD008771, 2008.
- Haefele, A., De Wachter, E., Hocke, K., Kampfer, N., Nedoluha, G. E., Gomez, R. M., Eriksson, P., Forkman, P., Lambert, A., and Schwartz, M. J.: Validation of ground-based microwave radiometers at 22 GHz for stratospheric and mesospheric water vapor, *J. Geophys. Res.*, 114, D23305, doi:10.1029/2009JD011997, 2009.
- Harris, N. R. P., Lehmann, R., Rex, M., and von der Gathen, P.: A closer look at Arctic ozone loss and polar stratospheric clouds, *Atmos. Chem. Phys.*, 10, 8499–8510, doi:10.5194/acp-10-8499-2010, 2010.
- Hoffmann, C. G., Raffalski, U., Palm, M., Funke, B., Golchert, S. H. W., Hochschild, G., and Notholt, J.: Observation of stratospheric CO above Kiruna with ground-based microwave radiometry – retrieval and satellite comparison, *Atmos. Meas. Tech.*, 4, 2389–2408, doi:10.5194/amt-4-2389-2011, 2011.

- Jiang, Y. B., Froidevaux, L., Lambert, A., Livesey, N. J., Read, W. G., Waters, J. W., Bojkov, B., Leblanc, T., McDermid, I. S., Godin-Beekmann, S., Filipiak, M. J., Harwood, R. S., Fuller, R. A., Daffer, W. H., Drouin, B. J., Cofield, R. E., Cuddy, D. T., Jarnot, R. F., Knosp, B. W., Perun, V. S., Schwartz, M. J., Snyder, W. V., Stek, P. C., Thurstans, R. P., Wagner, P. A., Allaart, M., Andersen, S. B., Bodeker, G., Calpini, B., Claude, H., Coetzee, G., Davies, J., De Backer, H., Dier, H., Fujiwara, M., Johnson, B., Kelder, H., Leme, N.P., Konig-Langlo, G., Kyrö, E., Laneve, G., Fook, L. S., Merrill, J., Morris, G., Newchurch, M., Oltmans, S., Parrondos, M. C., Posny, F., Schmidlin, F., Skrivankova, P., Stubi, R., Tarasick, D., Thompson, A., Thouret, V., Viatte, P., Vomel, H., von der Gathen, P., Yela, M., and Zabolocki, G.: Validation of the Aura Microwave Limb Sounder Ozone by Ozonesonde and Lidar Measurements, *J. Geophys. Res.*, 112, D24S34, doi:10.1029/2007JD008776, 2007.
- Larsen, N., Knudsen, B. M., Rosen, J. M., Kjome, N. T., Neuber, R., and Kyrö, E.: Temperature histories in liquid and solid polar stratospheric cloud formation, *J. Geophys. Res.*, 102, 23505–23517, 1997.
- Larsen, N., Mikkelsen, I. S., Knudsen, B. M., Schreiner, J., Voigt, C., Mauersberger, K., Rosen, J. M., and Kjome, N. T.: Comparison of chemical and optical in situ measurements of polar stratospheric clouds, *J. Geophys. Res.*, 105, 1491–1502, 2000.
- Livesey, N. J., Snyder, W. V., Read, W. G., and Wagner, P. A.: Retrieval algorithms for the EOS Microwave Limb Sounder (MLS) instrument, *IEEE T. Geosci. Remote*, 44, 1144–1155, 2006.
- Livesey, N. J., Filipiak, M. J., Froidevaux, L., Read, W. G., Lambert, A., Santee, M. L., Jiang, J. H., Pumphrey, H. C., Waters, J. W., Cofield, R. E., Cuddy, D. T., Daffer, W. H., Drouin, B. J., Fuller, R. A., Jarnot, R. F., Jiang, Y. B., Knosp, B. W., Li, Q. B., Perun, V. S., Schwartz, M. J., Snyder, W. V., Stek, P. C., Thurstans, R. P., Wagner, P. A., Avery, M., Browell, E. V., Cammas, J.-P., Christensen, L. E., Diskin, G. S., Gao, R.-S., Jost, H.-J., Loewenstein, M., Lopez, J. D., Nedelec, P., Osterman, G. B., Sachse, G. W., and Webster, C. R.: Validation of Aura Microwave Limb Sounder O<sub>3</sub> and CO observations in the upper troposphere and lower stratosphere, *J. Geophys. Res.*, 113, D15S02, doi:10.1029/2007JD008805, 2008.
- Livesey, N. J., Read, W. G., Froidevaux, L., Lambert, A., Manney, G. L., Pumphrey, H. C., Santee, M. L., Schwartz, M. J., Wang, S., Cofield, R. E., Cuddy, D. T., Fuller, R. A., Jarnot, R. F., Jiang, J. H., Knosp, B. W., Stek, P. C., Wagner, P. A., and Wu, D. L.: Earth Observing System (EOS) Aura Microwave Limb Sounder (MLS) Version 3.3 Level 2 data quality and description document, available at: <http://mls.jpl.nasa.gov/data/datadocs.php> (last access: 20 February 2013), 2011.
- Manney, G. L., Santee, M. L., Rex, M., Livesey, N. J., Pitts, M. C., Veefkind, P., Nash, E. R., Wohltmann, I., Lehmann, R., Froidevaux, L., Poole, L. R., Schoeberl, M. R., Haffner, D. P., Davies, J., Dorokhov, V., Gernandt, H., Johnson, B., Kivi, R., Kyrö, E., Larsen, N., Levelt, P. F., Makshtas, A., McElroy, C. T., Nakajima, H., Parrondo, M. C., Tarasick, D. W., von der Gathen, P., Walker, K. A., and Zinoviev, N. S.: Unprecedented Arctic ozone loss in 2011, *Nature*, 478, 469–475, doi:10.1038/nature10556, 2011.
- Muscari, G., Santee, M. L., and de Zafra, R. L.: Intercomparison of stratospheric HNO<sub>3</sub> measurements over Antarctica: Ground-Based Millimeter-wave versus UARS/MLS Version 5 retrievals, *J. Geophys. Res.*, 107, 4809, doi:10.1029/2002JD002546, 2002.
- Muscari, G., di Sarra, A. G., de Zafra, R. L., Lucci, F., Baordo, F., Angelini, F., and Fiocco, G.: Middle atmospheric O<sub>3</sub>, CO, N<sub>2</sub>O, HNO<sub>3</sub>, and temperature profiles during the warm Arctic winter 2001–2002, *J. Geophys. Res.*, 112, D14304, doi:10.1029/2006JD007849, 2007.
- Muscari, G., Cesaroni, C., Fiorucci, I., Smith, A. K., Froidevaux, L., and Mlynczak, M. G.: Strato-mesospheric ozone measurements using ground-based millimeter-wave spectroscopy at Thule, Greenland, *J. Geophys. Res.*, 117, D07307, doi:10.1029/2011JD016863, 2012.
- Nedoluha, G. E., Gomez, R. M., Hicks, B. C., Helmboldt, J., Bevilacqua, R. M., and Lambert, A.: Ground-based microwave measurements of water vapor from the midstratosphere to the mesosphere, *J. Geophys. Res.*, 116, D02309, doi:10.1029/2010JD014728, 2011.
- Palm, M., Hoffmann, C. G., Golchert, S. H. W., and Notholt, J.: The ground-based MW radiometer OZORAM on Spitsbergen – description and status of stratospheric and mesospheric O<sub>3</sub>-measurements, *Atmos. Meas. Tech.*, 3, 1533–1545, doi:10.5194/amt-3-1533-2010, 2010.
- Parrish, A., de Zafra, R. L., Solomon, P. M., and Barrett, J. W.: A ground-based technique for millimeter wave spectroscopic observations of stratospheric trace constituents, *Radio Sci.*, 23, 106–118, 1988.
- Parrish, A., Connor, B. J., Tsou, J. J., McDermid, I. S., and Chu, W. P.: Ground-Based Microwave Monitoring of Stratospheric Ozone, *J. Geophys. Res.*, 97, 2541–2546, doi:10.1029/91JD02914, 1992.
- Pickett, H. M., Poynter, R. L., Cohen, E. A., Delitsky, M. L., Pearson, J. C., and Müller, H. S. P.: Submillimeter, millimeter, and microwave spectral line catalog, *J. Quant. Spectrosc. Ra.*, 60, 883–890, doi:10.1016/S0022-4073(98)00091-0, 1998.
- Rex, M., Salawitch, R. J., Deckelmann, H., von der Gathen, P., Harris, N. R. P., Chipperfield, M. P., Naujokat, B., Reimer, E., Allaart, M., Andersen, S. B., Bevilacqua, R., Braathen, G. O., Claude, H., Davies, J., De Backer, H., Dier, H., Dorokhov, V., Fast, H., Gerding, M., Godin-Beekmann, S., Hoppel, K., Johnson, B., Kyrö, E., Litynska, Z., Moore, D., Nakane, H., Parrondo, M. C., Risley Jr., A. D., Skrivankova, P., Stubi, R., Viatte, P., Yushkov, V., and Zerefos, C.: Arctic winter 2005: Implications for stratospheric ozone loss and climate change, *Geophys. Res. Lett.*, 33, L23808, doi:10.1029/2006GL026731, 2006.
- Rodgers, C. D.: Retrieval of atmospheric temperature and composition from remote measurements of thermal radiation, *Rev. Geophys. Space Ge.*, 14, 609–624, 1976.
- Rodgers, C. D.: Inverse method for atmospheric sounding, Series on atmospheric, oceanic and Planetary Physics – Vol. 2, edited by Taylor, F. W., World Scientific Publishing Co. Pte Ltd, Singapore, 2000.
- Rothman, L. S., Gordon, I. E., Barbe, A., ChrisBenner, D., Bernath, P. F., Birk, M., Boudon, V., Brown, L. R., Campargue, A., Champion, J.-P., Chance, K., Coudert, L. H., Dana, V., Devi, V. M., Fally, S., Flaud, J.-M., Gamache, R. R., Goldman, A., Jacquemart, D., Kleiner, I., Lacome, N., Lafferty, W. J., Mandin, J.-Y., Massie, S. T., Mikhailenko, S. N., Miller, C. E., Moazzen-Ahmadi, N., Naumenko, O. V., Nikitin, A. V., Orphal, J., Perevalov, V. I., Perrin, A., Predoi-Cross, A., Rinsland, C. P., Rotger, M., Šimečková, M., Smith, M. A. H., Sung, K., Tashkun, S. A., Tennyson, J., Toth, R. A., Vandaele, A. C., and Van der Auw-

- era, J.: The HITRAN 2008 molecular spectroscopic database, *J. Quant. Spectrosc. Ra.*, 110, 533–572, 2009.
- Santee, M. L., Lambert, A., Read, W. G., Livesey, N. J., Cofield, R. E., Cuddy, D. T., Daffer, W. H., Drouin, B. J., Froidevaux, L., Fuller, R. A., Jarnot, R. F., Knosp, B. W., Manney, G. L., Perun, V. S., Snyder, W. V., Stek, P. C., Thurstans, R. P., Wagner, P. A., Waters, J. W., Muscari, G., deZafra, R. L., Dibb, J. E., Fahey, D. W., Popp, P. J., Marcy, T. P., Jucks, K. W., Toon, G. C., Stachnik, R. A., Bernath, P. F., Boone, C. D., Walker, K. A., Urban, J., and Murtagh, D.: Validation of Aura Microwave Limb Sounder HNO<sub>3</sub> Measurements, *J. Geophys. Res.*, 112, D24S40, doi:10.1029/2007JD008721, 2007.
- Schoeberl, M. R., Douglass, A. R., Hilsenrath, E., Bhartia, P. K., Barnett, J., Beer, R., Waters, J., Gunson, M., Froidevaux, L., Gille, J., Levelt, P. F., and DeCola P.: Overview of the EOS Aura Mission, *IEEE T. Geosci. Remote*, 44, 1066–1074, 2006.
- Solomon, S.: Progress towards a quantitative understanding of Antarctic ozone depletion, *Nature*, 347, 347–354, doi:10.1038/347347a0, 1990.
- Twomey, S.: Introduction to the Mathematics of Inversion in Remote Sensing and Indirect Measurements, *Developments in Geomathematics*, Vol. 3, Elsevier Scientific Publ., Amsterdam, 1977.
- Twomey, S., Herman, B., and Rabinoff, R.: An extension of the Chahine method of inverting the radiative transfer equation, *J. Atmos. Sci.*, 34, 1085–1090, 1977.
- Waters, J. W., Froidevaux, L., Read, W. G., Manney, G. L., Elson, L. S., Flower, D. A., Jarnot, R. F., and Harwood, R. S.: Stratospheric ClO and ozone from the Microwave Limb Sounder on the Upper Atmosphere Research Satellite, *Nature*, 362, 597–602, 1993.
- Waters, J. W., Froidevaux, L., Harwood, R. S., Jarnot, R. F., Pickert, H. M., Read, W. G., Siegel, P. H., Cofield, R. E., Filipiak, M. J., Flower, D. A., Holden, J. R., Lau, G. K., Livesey, N. J., Manney, G. L., Pumphrey, H. C., Santee, M. L., Wu, D. L., Cuddy, D. T., Lay, R. R., Loo, M. S., Perun, V. S., Schwartz, M. J., Stek, P. C., Thurstans, R. P., Boyles, M. A., Chandra, K. M., Chavez, M. C., Chen, G.-S., Chudasama, B. V., Dodge, R., Fuller, R. A., Girard, M. A., Jiang, J. H., Jiang, Y., Knosp, B. W., LaBelle, R. C., Lam, J. C., Lee, K. A., Miller, D., Oswald, J. E., Patel, N. C., Pukala, D. M., Quintero, O., Scaff, D. M., Snyder, W. V., Tope, M. C., Wagner, P. A., and Walch, M. J.: The Earth Observing System Microwave Limb Sounder (EOS MLS) on the Aura Satellite, *IEEE T. Geosci. Remote*, 44, 1075–1092, 2006.
- WMO (World Meteorological Organization), Scientific Assessment of Ozone Depletion: 2010, Global Ozone Research and Monitoring Project-Report No. 52, 516 pp., Geneva, Switzerland, 2011.